ACS OMEGA

Article

Cite This: ACS Omega 2018, 3, 13772−13781

http://pubs.acs.org/journal/acsodf

Flexible Optical Amplifier for Visible-Light Communications Based on Organic−Inorganic Hybrids

Ana Bastos,[†,‡] Barry McKenna,[§] Mário Lima,[‡] Paulo S. André,[∥] Luís D. Carlos,[†] Rachel C. Evans,[⊥] and Rute A. S. Ferreira*[,†]

[†]Department of Physics, CICECO—Aveiro Institute of Materials and [‡]Department of Electronics, Telecommunications and Informatics, Instituto de Telecomunicações, University of Aveiro, Campus Universitário de Santiago, 3810-193 Aveiro, Portugal

[§]School of Chemistry, Trinity College Dublin, Dublin 2, Ireland

[∥]Instituto de Telecomunicações and Department of Electric and Computer Engineering, Instituto Superior Técnico, Universidade de Lisboa, Avenida Rovisco Pais, 1049-001 Lisbon, Portugal

[⊥]Department of Materials Science & Metallurgy, University of Cambridge, 27 Charles Babbage Road, Cambridge CB3 0FS, U.K.

Supporting Information

ABSTRACT: Visible-light communications (VLCs) based on white light-emitting diodes (LEDs) are emerging as a low-cost and energy-efficient alternative solution to wireless communications. As white emitting LEDs use a combination of a long-lived yellow emission combined with the faster response of a blue emitting LED (~460 nm), VLC technology requires amplification of the blue component to improve the signal-to-noise ratio. We report the fabrication and characterization of planar and channel waveguides based on a blue-emitting polyfluorene conjugated polyelectrolyte, namely, poly[9,9-bis(4-sulfonylbutoxyphenyl)fluorene-2,7-diyl-*alt*-1,4-phenylene] (PBS-PFP) incorporated into diureasil organic−inorganic hybrids for optical amplification in VLC. Taking advantage of the diureasil host as a UV self-patternable material, direct UV laser writing was used to pattern channel waveguides with a larger refractive index (Δn=0.09) compared to the nonexposed region, enabling confinement and guidance of the PBS-PFP emission with a maximum optical gain efficiency value of 1.62 ± 0.02 cm μJ^{-1}. This value is among the best figures of merit known for polymeric materials with additional advantages added by the diureasil hybrid host, namely, mechanical flexibility, thermal stability, and low insertion losses due to the nearly null refractive index contrast between the optical fiber and the amplification device, establishing the proposed approach as a promising cost-effective solution for optical amplification in VLCs.

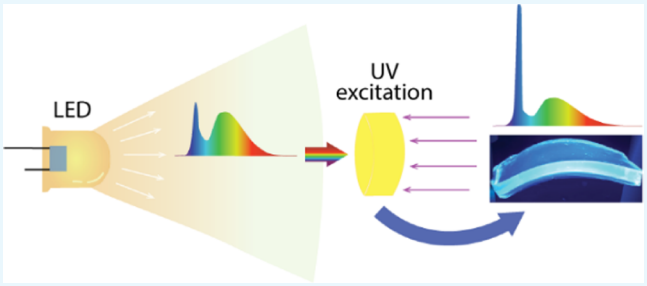

INTRODUCTION

Recent advances in light-emitting diode (LED) technology have created a new generation of energy-efficient light sources that look set to revolutionize the indoor lighting market.[1] Modern LEDs can be rapidly modulated, presenting opportunities for their future application in visible-light communications (VLCs), in which the LED simultaneously functions as a light source and wireless signal transmitter to transfer information at rates up to gigabits per second.[2] While inorganic materials have traditionally dominated the fields of solid-state lighting and optical communications, organic materials are rapidly emerging as alternatives for applications where inorganics are not ideally suited, such as those requiring large active areas, color tunability, or mechanical flexibility.[3−5] The wide-scale commercial availability of organic-based LEDs is a prime example of how these key attributes can be successfully leveraged.[6,7]

White-light emitting LEDs for VLC can be produced in two ways: a combined red−green−blue LED module, or alternatively, a blue LED is coated with a phosphor color converter.[8] Conjugated polymers (CPs) have recently been successfully implemented as organic color converters to replace traditional inorganic phosphor coatings.[9−11] High absolute photoluminescence quantum yields (PLQYs), tunable emission colors, and in particular, subnanosecond emission lifetimes make CPs attractive for this purpose, since these features enable higher communication bandwidths to be attained than for conventional inorganic phosphors, which emit in the micro-millisecond regime.[12] Conjugated polymers have also been used to prepare freestanding polymer membrane lasers[13] or have been doped within polymer organic fibers or slab waveguides to generate waveguide modulators[14] and optical amplifiers.[15−18] The latter operation was already demonstrated for optical fiber communications, where the infrared spectral component (1.3−1.5 μm) was amplified.[19,20]

Received: July 20, 2018
Accepted: September 25, 2018
Published: October 22, 2018

DOI: 10.1021/acsomega.8b01726
ACS Omega 2018, 3, 13772−13781

For VLC, optical amplifiers are usually required to enhance the blue component of the transmitting signal.[2]

Despite the ease of processability, the simultaneous control of both the morphology and electronic properties remains a significant challenge for conjugated polymers. Optical loss mechanisms, such as singlet-state annihilation and charge generation, are mediated by interchain coupling,[21] which becomes exacerbated upon transfer to the solid state. Strategies for the control of intermolecular interactions, while maintaining or even enhancing the optical properties in the solid-state are thus highly desirable. We have recently shown that incorporation of CPs into organosilica hybrid polymers known as diureasils (Figure 1) is an effective approach to minimize interchain interactions leading to highly emissive solid-state materials.[22,23]

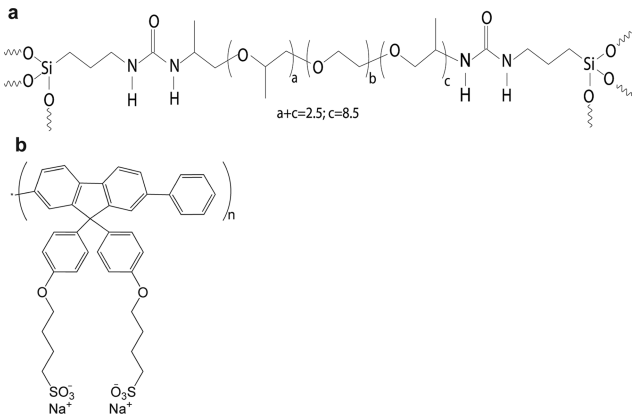

Figure 1. Molecular structures of (a) diureasil (dU(600)) and (b) poly[9,9-bis(4-sulfonylbutoxyphenyl)fluorene-2,7-diyl-*alt*-1,4-phenylene] (PBS-PFP).

Moreover, diureasils are intrinsically photoluminescent, emitting in the purple−blue spectral region with a lifetime of nano-microseconds,[24,25] and have a reasonable refractive index ($n \sim 1.5$[26]), which enables them to be used as waveguides for optical amplification,[27] high-rejection optical filters,[28] and luminescent solar concentrators.[29−33] Diureasils also offer acceptable absorption values (1−5 dB cm^{-1} at 1550 nm) and low insertion losses due to fiber−device refractive index mismatch.[26] Electronic coupling between the CP and the ureasil, combined with the formation of isolated polymer domains, leads to the creation of localized radiative trap sites, which relax with a PLQY of >0.60.[22]

Inspired by these results, we postulated that the combination of a short-lived CP, coupled with the waveguide characteristics of the diureasil, could deliver a fast-response optical amplifier, suitable for VLC. To minimize spectral losses, we chose to use the blue-emitting poly[9,9-bis(4-sulfonylbutoxyphenyl)-fluorene-2,7-diyl-*alt*-1,4-phenylene] (PBS-PFP, Figure 1), which exhibits good spectral overlap with the diureasil and shows thermally assisted population of radiative trap sites.[22] PBS-PFP is also water-soluble, thus affording good compatibility with the aqueous sol−gel conditions used to fabricate the diureasil (dU(600)). Moreover, we exploit the intrinsic self-patternability of diureasils to fabricate optical architectures within the CP−diureasil composites using direct UV laser writing on the surface.[34] We demonstrate that this multi-pronged approach results in low-cost organic−inorganic hybrid linear waveguides, which exhibit a maximum optical gain efficiency of 1.62 ± 0.02 cm μJ^{-1}.

RESULTS AND DISCUSSION

Organic−inorganic hybrid materials incorporating PBS-PFP have been synthesized by the versatile sol−gel methodology at ambient temperature. Monolithic PBS-PFP diureasils are flexible, transparent under daylight, and exhibit an intense blue emission under UV radiation (365 nm), as shown in Figure 2a. The transparency was quantified by the

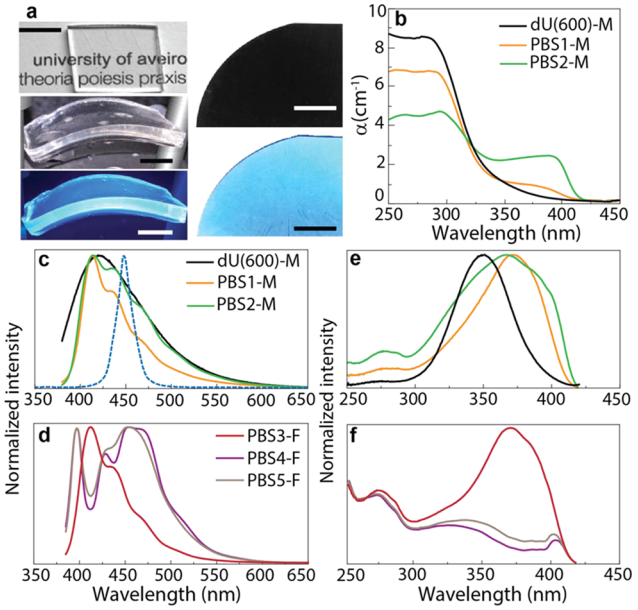

Figure 2. Absorption and photoluminescence properties of PBS-PFP-diureasil monoliths and films. (a) Photographs of the flexible PBS2-M monolith (left) and PBS5-F film (right) taken under daylight (top) and ultraviolet illumination (bottom). The scale bars represent 1 cm. (b) UV/vis absorption coefficient (α) spectral dependence for monoliths and the dU(600). (c, d) Emission spectra excited at 365 nm and (e, f) the corresponding excitation spectra monitored at 435 nm for monoliths (M) and films (F). The dashed line represents the typical emission of the commercial InGaN-based LED used to produce the commercial solid-state LEDs.[37]

measurement of the absorption coefficient (α) from the UV/vis absorption spectra that comprise a main absorption band in the UV region (250−325 nm), assigned to the dU(600) host[35] (Figure 2b), with a maximum absorption coefficient of ∼8.5 cm^{-1}. After doping with PBS-PFP, although the host-related absorption band still dominates the spectra, α decreases to around ∼6.7 and ∼4.5 cm^{-1} for PBS-1 and PBS-2, respectively. Moreover, upon increasing the PBS-PFP concentration, a new band peaking at 380 nm appears, which is ascribed to the polyfluorene absorption.[36] For all samples, for wavelengths longer than 400 nm, α is very low (<0.1 cm^{-1}), providing transparency under daylight.

Upon excitation at 365 nm, PBS-PFP diureasil monoliths reveal a structured emission band between 390 and 550 nm (Figure 2c), which is characteristic of the vibronic relaxation of the polyfluorene excited singlet state.[30] However, the contribution of the intrinsic emission of dU(600)[35] to the spectrum cannot be neglected as it also occurs in the same spectral region (Figure 2c). Comparing the emission spectra of the samples processed as monoliths with those in films (Figure

DOI: 10.1021/acsomega.8b01726
ACS Omega 2018, 3, 13772−13781

2d), while those for the low-concentrated film (PBS-3-F) resemble the emission spectra of the monoliths, the emission spectra of the more concentrated films (PBS4-F and PBS-5-F) are shifted to the blue region, revealing additional variations in the relative intensity of the vibronic progression components. In any case, we note that as desirable for VLC, the blue emission of the PBS-PFP diureasils overlaps that of the InGaN-based LED used to produce the commercial solid-state LEDs, whose white light results from the mixture of the blue emission arising from high-efficiency LEDs and yellow-emitting YAG:Ce phosphor.[38]

The contribution of both the dU(600) and PBS-PFP excited states to the observed blue emission is also inferred from the excitation spectra monitored around 435 nm (Figure 2e,f). The spectra are dominated by a band between 300 and 450 nm, assigned to overlapping contributions from PBS-PFP and the dU(600) host, and a weaker component around 275 nm. However, variations in the relative intensity and bandwidth of the peaks are observed as a function of the PBS-PFP wt %. As noted above for the more concentrated films, the excitation spectra differ from those of the monoliths and the low-concentration film. These observations can be attributed to a combination of factors. First, the processing methodology used can lead to distinct kinetic control of the sol−gel process, in particular differences in the gelation times (hours for the bulk and seconds for the films), which is known to modulate the degree of organization of the dU(600) host material.[39−41] Thus, both the monolithic and film samples are expected to provide a distinct host environment for the PBS-PFP chains. Second, while PBS-PFP is soluble in dilute solutions of mixed polar solvents (such as the tetrahydrofuran (THF)/water mixture used to prepare the samples), it tends to form dispersions of supramolecular aggregates in pure water.[42,43] Thus, preferential evaporation of THF during the gelation and drying processing steps will gradually induce a local concentration gradient in the samples, leading to an increasingly more aqueous environment, in which chain entanglements will be favored. This process will occur more rapidly for the films and for samples with a higher PBS-PFP wt %, although electrostatic/polar interactions with diureasil and other siliceous hosts have been shown to control the extent of aggregation of conjugated polymers at the organic−inorganic interface.[30,44,45] From Figure 2e,f, at the lowest PBS-PFP concentration in both the film (PBS3-F) and monolith (PBS1-M) samples, the excitation and emission spectra are reminiscent of well-dissolved PBS-PFP chains, with some excitation of the PBS-PFP emission arising from energy transfer from the dU(600) host.[22] As the concentration is increased in the monoliths (e.g., PBS2-M), the excitation spectrum indicates an increase in the electronic interaction between the host−guest species, while the band broadening and change in the vibronic structure in the emission spectrum suggest increasing aggregation of the PBS-PFP chains. In the film samples, the effect of aggregation becomes even more apparent, with the red shift in the emission band and change in the relative intensity of the vibronic peaks indicative of self-absorption (usually designated as inner-filter effect).[46]

The photoluminescence quantum yields obtained on excitation at 365 nm are shown in Table 1 and reveal a significant increase as a function of increasing PBS-PFP wt %, reaching 0.411 ± 0.005 and 0.759 ± 0.008 for PBS1-M and PBS2-M, respectively. Independently of the concentration, the films reveal lower photoluminescence quantum yield values in comparison to those found for the monoliths, despite the same trend of increase being observed with the PBP-PFP wt %, achieving a maximum value of (0.011 ± 0.001) for PBS5-F. The dU(600) monolith exhibits a PLQY of 0.179 ± 0.002, which is in good agreement with previously reported values.[22] The increase in PLQY with the concentration reflects the significant contribution of the PBS-PFP to the photoluminescence as the host reveals intrinsically lower values. This enhanced PLQY in the blue spectral region renders it easier to excite the samples using commercial UV-emitting LEDs, showing the potential of the material to be integrated with VLC as an optical amplifier.

Table 1. Sample Composition, thickness and absolute photoluminescente quantum yield (PLQY) PBS Diureasils[a]

sample	wt % PBS-PFP	thickness (mm)	PLQY[b]
dU(600)-M	0	2.9	0.179
PBS1-M	1.2×10^{-3}	2.7	0.411
PBS2-M	1.2×10^{-2}	3.2	0.759
dU(600)-F	0	0.8×10^{-3}	0.001
PBS3-F	2.5×10^{-2}	3.3×10^{-3}	0.004
PBS4-F	0.2	1.6×10^{-3}	0.010
PBS5-F	0.2	1.8×10^{-3}	0.011

[a]The weight percent of polymer incorporated was estimated from [PBS-PFP] and the resultant mass of the dry PBS-PFP diureasil. M and F denote monolith and film samples, respectively. [b]The error is estimated to be 10% of the PLQY (see Methods for details).

To further characterize the optical features of these materials, the refractive index (n) was monitored by spectroscopic ellipsometry. The measured ellipsometric parameters I_s and I_c and the respective fits are represented in Figure S1 (Supporting Information (SI)). The resulting dispersion curves are shown in Figure 3a and show that the refractive index increases with PBS-PFP wt %, yielding a refractive index difference at 450 nm of +0.01 between PBS2-M and dU(600) and of +0.02 between PBS5-F and dU(600). The increase in the refractive index upon addition of PBS-PFP is expected as conjugated polymers are known to have a refractive index value >1.6,[47] larger than that of the nondoped dU(600).[26,48]

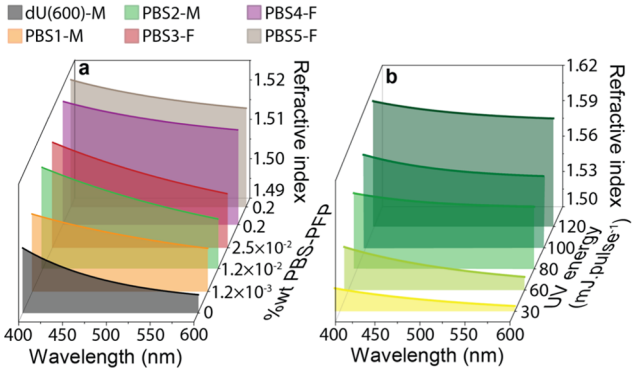

Figure 3. Optical properties of pristine and UV-exposed PBS-PFP diureasils. Dispersion curves for (a) pristine monolithic and film samples and (b) channel waveguides in PBS2-M as a function of the laser pulse energy used in the writing system (30−120 μJ pulse^{-1}).

As mentioned above, one of the advantages of using the diureasil organic−inorganic hybrid as a host is the possibility to locally control the refractive index through UV exposure by

DOI: 10.1021/acsomega.8b01726
ACS Omega 2018, 3, 13772−13781

direct writing with a UV pulsed laser.[26] Taking this feature into account, n was studied as a function of the UV pulsed laser energy (μJ pulse^{-1}) through ellipsometric measurements in the exposed regions. The measured ellipsometric parameters I_s and I_c, and the respective fits are represented in Figures S2 and S3 (Supporting Information). As an illustrative example, Figure 3b presents the dispersion curves for UV-exposed regions of PBS2-M, revealing a refractive index increase with the UV dose used in the exposition. A positive refractive index contrast between the exposed and nonexposed regions (Δn) was observed, yielding a maximum Δn of +0.09, at 450 nm, for a UV dose of ~120 μJ pulse^{-1}. The dispersion curves for the exposed regions in PBS1-M (Figure S4, Supporting Information) also reveal a positive refractive index contrast, yielding a maximum value for Δn of +0.03 at 450 nm. Thus, the refractive index of the PBS-PFP-based diureasils can be easily tuned through chemical (PBS-PFP doping) and physical (UV exposure) parameters, in which the UV-exposed region can be assumed to behave as channel waveguides. Then, using UV laser writing, channel waveguides were patterned on the surface of the monoliths, yielding a length of ~2×10^{-2} m and a width of ~2.00×10^{-4} m. An optical microscopy image of a channel waveguide written with 120 μJ pulse^{-1} on the PBS2-M surface under UV illumination is shown in Figure 4b. We note that the thin films, without UV exposure, behave as planar waveguides, where the propagation occurs without lateral confinement.

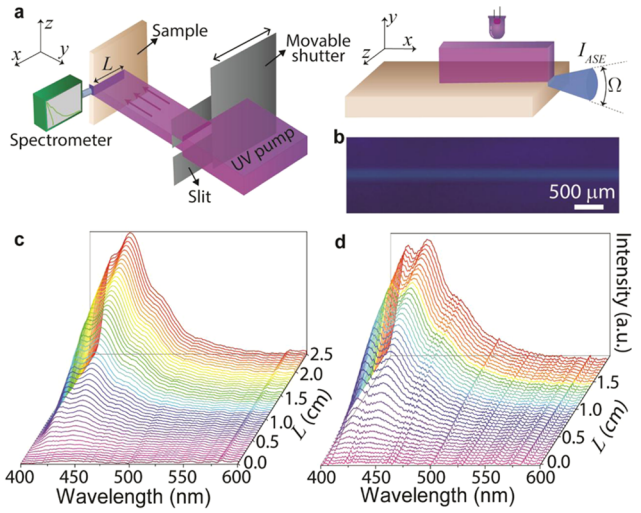

Figure 4. Determination of the optical gain in PBS-PFP diureasils using the variable stripe length (VSL) technique. (a) Schematic representation of the experimental setup used for the variable stripe length measurements. (b) Optical microscopy image showing the channel waveguide written with 120 μJ pulse^{-1} on the PBS2-M surface, under UV radiation. (c, d) Emission spectra for different stripe lengths in the planar waveguide PBS2-M and channel waveguide written with 120 μJ pulse^{-1} on the surface of PBS2-M, respectively.

Since these materials have a high PLQY and show a positive Δn, the optical gain was measured by applying the variable stripe length technique in the planar and channel waveguides, using the experimental setup represented in Figure 4a. The emission spectra were acquired for a stripe length range of 0.0−2.5 × 10^{-2} m, with a step of 5 × 10^{-4} m. As a representative example, Figure 4c,d shows the amplified spontaneous emission (ASE) spectra for the planar waveguide PBS2-M and for the channel waveguide written with 120 μJ pulse^{-1} on PBS2-M.

Figure 5a,b shows the respective ASE integrated intensity versus the stripe length for the planar and channel waveguides

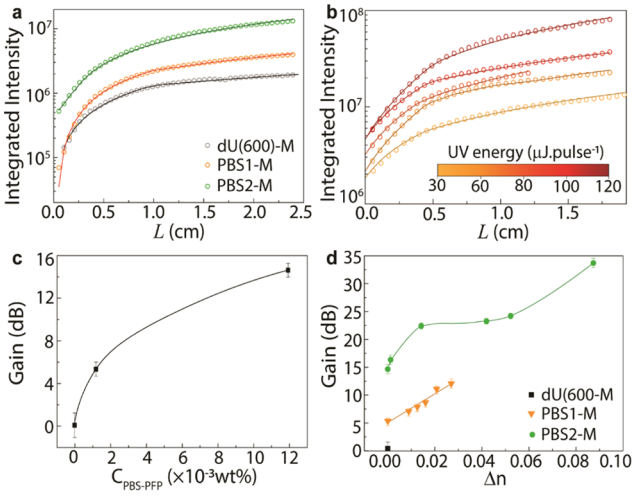

Figure 5. (a, b) Integrated ASE intensity as a function of the stripe length for the planar waveguides, and the channel waveguides written on the PBS2-M surface, respectively. Calculated optical gain coefficients as a function of (c) PBS-PFP concentration (wt %) in the diureasil, and (d) refractive index contrast (Δn) at 450 nm between the channel and planar waveguides regions.

produced with PBS2-M. The emission spectra and the respective integrated intensity for PBS1-M and the channels written in PBS1-M and PBS2-M are in Figures S5−S8 (Supporting Information). An increase in the ASE emission with the excitation length is clearly observed. This behavior can be described by a one-dimensional optical amplifier rod, where the propagation equation for the ASE intensity, I_{ASE}, taking into account the gain saturation, can be written as[49]

$$\frac{dI_{ASE}}{dz} = \frac{g_0 \cdot I_{ASE}}{1 + \frac{I_{ASE}(z)}{I_{sat}}} + \left(A_{sp} \frac{N_0^*}{1 + \frac{I_{ASE}(z)}{I_{sat}}} \times h\nu \right) \times [\Omega/4\pi] \quad (1)$$

where g_0 is the optical gain coefficient, I_{sat} is the signal saturation intensity, A_{sp} is the spontaneous emission rate, N_0* is the excited-state population density, and $h\nu$ is the energy of the emitted photon.[49] Ω is the solid angle defined by the output side of the amplifier and the slit on the sample surface (Figure 4a), and for simplicity, it is set to be constant.[49] Integration of eq 1 leads to eq 2, from which it is possible to extract the optical gain coefficient by the fitting to the experimental data.

$$I_{ASE} = \frac{(g_0 I_{sat} - J_{sp})}{g_0} W\left(\frac{e^{g_0 z}}{g_0 I_{sat} - J_{sp}} (J_{sp}\, e^{J_{sp}/g_0 I_{sat} - J_{sp}})^{1-(J_{sp}/g_0 I_{sat} - J_{sp})} \right) - \frac{J_{sp}}{g_0} \quad (2)$$

DOI: 10.1021/acsomega.8b01726
ACS Omega 2018, 3, 13772−13781

where $J_{sp} = \left(\frac{A_{sp} h\nu \Omega N^*}{4\pi}\right)$ is the intensity of the spontaneous emission and W is the Lambert function. The gain values obtained for the planar waveguide monoliths are represented in Figure 5c, which show an increase of the optical gain values by increasing the polymer concentration in the diureasil. The maximum optical gain obtained was 15.0 ± 0.2 dB (35.0 ± 0.1 cm^{-1}) for PBS2-M.

Using the same approach, the optical gain coefficient was also calculated for the channel waveguides. Figure 5d shows the optical gain values obtained for the channel waveguides written on PBS1-M and PBS2-M surfaces, which reveals an increase in gain with increase in Δn. The maximum gain obtained was ∼34.0 ± 0.2 dB (78.0 ± 0.1 cm^{-1}) for the channel with Δn = 0.09 in PBS2-M. The gain increase in the channel waveguide samples results from the confinement of the radiation, and therefore by the increase of the population inversion. Concluding, similarly to the refractive index, the optical gain can also be defined through chemical (PBS-PFP doping) and physical (UV exposure) parameters.

Furthermore, to assess the optical propagation and net gain in the channel waveguide, a probe optical signal (λ = 450 nm) was coupled to the channel input. Signal propagation through the waveguide was attained, and an optical fiber was aligned to the channel output extremity to measure the output emission spectra, using a spectrometer. As a representative example, Figure 6a shows the spectra obtained at the output for the channel waveguide with Δn = 0.09 in PBS2-M. The spectra were taken, independently, without pump excitation, and with UV excitation through an external perpendicular pump source placed above the channel waveguide, and a UV pump co-propagating with the probe optical signal. From the spectra, an intensity improvement was observed when the waveguide was excited, especially for external perpendicular pumping. The spectra obtained at the waveguide output for PBS1-M and PBS2-M are represented in Figure S9 (Supporting Information), and also reveal an improvement in the emission intensity when the waveguide was excited.

To further evaluate the channel waveguides, the net optical gain (dB) was calculated. The probe optical signal was modulated in intensity with a square waveform (50% duty cycle) at 200 Hz using a mechanical chopper. The output signal was detected by a photodiode connected to an oscilloscope. As an example, the signal transmitted in the waveguide with Δn = 0.09 in PBS2-M is represented in Figure 6b without pumping, with external perpendicular pumping, and with co-propagation pumping. Again, an improvement in the intensity is observed when the waveguide is exposed to UV radiation, mainly when the excitation is external. The net gain values were estimated from the ratio between the peak-to-peak voltages of the received signal with and without pumping. Using the two pumping approaches, the maximum gain observed was in the waveguide with the higher refractive index contrast (Δn = 0.09), yielding values of ∼32 and ∼16 dB, with external and with co-propagation pumping, respectively (Figure 6c). The received signals of the waveguides in PBS1-M and PBS2-M, and the respective net gain values for PBS1-M are represented in Figures S10 and S11 (Supporting Information).

The gain efficiency $\left(\eta_G = \frac{G}{\text{pump}}\right)$ was calculated, in which pump indicates either the pump signal energy density (η_G, μJ cm^{-2}) or power density (η'_G, kW cm^{-2}), to enable a comparison with previous studies reported in the literature.

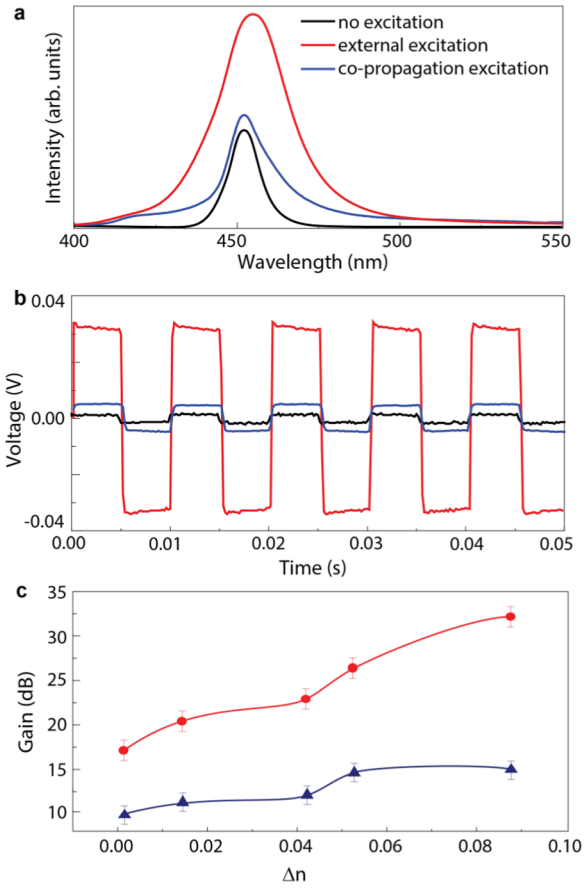

Figure 6. (a) Spectra at the channel waveguide output with Δn = 0.09 in PBS2-M. (b) Optical signal at the channel waveguide output with Δn = 0.09 in PBS2-M (the photodiode operates with an output capacitor, removing the DC component). (c) Gain calculated for each waveguide channel written on the PBS2-M surface, for planar excitation (red line) and co-propagation excitation (blue line).

In this work, light propagation and amplification was attained with high optical gain efficiency values that envisage application of the proposed devices for VLC applications. In particular, to the best of our knowledge, larger or similar optical gain values were only achieved for pure polydioctylfluorene (PFO)[50] and poly(9,9-dioctylfluorene-*co*-9,9-di(4-methoxy)phenylfluorene) (F8DP),[51] which has higher processing cost than our PBS-PFP-diureasil hybrid. We note that compared to other hybrid materials, the gain efficiency values obtained are among the best previously reported in the literature (Table 2). The highest gain efficiency values, calculated through the energy density, were 0.73 ± 0.01 and 1.62 ± 0.02 cm μJ^{-1} for planar (PBS2-M) and channel waveguides (Δn = 0.09 in PBS2-M), respectively, which are among the best values reported in the literature for pure polymers (Table 2).

As the gain efficiency values are comparable to those previously reported for both pure conjugated polymers and hybrid materials, PBS-PFP diureasils are a promising cost-effective solution for optical amplification in white light-emitting diodes for VLC.

DOI: 10.1021/acsomega.8b01726
ACS Omega 2018, 3, 13772−13781

Table 2. Excitation/Emission Wavelengths ($\lambda_{exc}/\lambda_{em}$), Optical Gain ($G$), Pump Energy, Pump Power Density, and the Corresponding Gain Efficiencies (η_G and η'_G) of Selected Polymer-Based Materials and Organic−Inorganic Hybrids[a]

			pump			gain efficiency	
	material	$\lambda_{exc}/\lambda_{em}$ (nm)	energy (μJ cm^{-2})	power density (kW cm^{-2})	G (cm^{-1})	η_G (cm μJ^{-1})	η'_G (cm kW^{-1})
planar	dU(600)/PBS-PFP	365/450	48.0 ± 0.5	2.40 ± 0.02	35.0 ± 0.1	0.73 ± 0.01	14.6 ± 0.2
	PM 650-PMMA[52]	532/620		23 × 10^3	12		5.2 × 10^{-4}
	fvin[53]	532/640	413		50	0.12	
	DCM-PMMA[53]				40	0.10	
	Coumarin-495[54]	−/534		7 × 10^3	3.5		5.0 × 10^{-4}
	F8DP[51]	355/452		0.6	66		110
	F8BT[51]	440/576		2.8	22		7.8
	Dow Red F[51]	440/685			24		8.6
	m-LPPP[55]	490/−		22	50		2.3
	BuEH-PPV[56]	435/562		1.2	18		15
				2.2	41		18.6
				4.1	62		15.1
	PFO[50]	−/466	9		74	8.2	
			1.3		10	7.7	
channel	dU(600)/PBS-PFP	365/450	48.0 ± 0.5	2.40 ± 0.02	78.0 ± 0.1	1.62 ± 0.02	32.5 ± 0.3

[a]PM 650-PMMA: pyrromethene 650 in poly(methyl methacrylate); fvin: (4-di(4′-*tert*-butylbiphenyl-4-yl)amino-4′-dicyanovinylbenzene); DCM: 4-dicyanomethylene-2-methyl-6-*p*-dimethylamino-styryl-4*H*-pyran; F8DP: poly(9,9-dioctylfluorene-*co*-9,9-di(4-methoxy)phenylfluorene); F8BT: poly(9,9-dioctylfluorene-*co*-benzo-thiadiazole); m-LPPP: methyl-substituted conjugated laddertype poly(paraphenylene); BuEH-PPV: poly[2-butyl-5-(2′-ethyl-hexyl)-1,4-phenylenevinylene]; and PFO: poly(9,9-dioctyl-fluorene).

CONCLUSIONS

Planar and channel waveguides based on PBS-PFP doped within diureasil organic−inorganic hybrids were fabricated and optically characterized with the view of their potential application as optical amplifiers for VLC based on white light-emitting diodes. From the efficient and synergetic energy transfer between the diureasil-excited states and those of the PBS-PFP, an enhanced high-efficiency and stable emission in the blue spectral region (peaking around 390−550 nm) occurs, which overlaps that of commercial solid-state LEDs used for VLC.

We give emphasis to the heavily facilitated control of the surface optical properties by the inherent flexibility offered by these materials that are easily self-patterned by UV exposition laser writing, in contrast to traditional lithographic processes. Therefore, the refractive index of the PBS-PFP-based diureasils can be facilely tuned through chemical (PBS-PFP doping) and physical (UV exposure) means. This characteristic was exploited to pattern channel waveguides on the surface of PBS-PFP diureasil monoliths using direct UV laser writing, and radiation confinement was observed.

The optical gain coefficient was measured using the variable stripe length method, showing an increase in optical gain with the PBS-PFP concentration and with the irradiated UV energy amount. To further evaluate the channel waveguides, the net gain was measured, using an optical signal peaking at 450 nm coupled in the input, transmitting bits, showing an intensity improvement when the waveguides were exposed to UV radiation.

The maximum gain efficiency value observed in planar waveguides was 0.73 ± 0.01 cm μJ^{-1} (14.6 ± 0.2 cm kW^{-1}), which corresponds to the sample with the highest PBS concentration (PBS2-M). In the channel waveguides, the highest gain efficiency obtained was 1.62 ± 0.02 cm μJ^{-1} (32.5 ± 0.3 cm kW^{-1}) for the channel with Δn = 0.09 in PBS2-M when it was excited above the channel.

These values are among the best known for conjugated polymers and hybrid materials. To the best of our knowledge, larger values were only achieved for pure PFO, which has a higher processing cost than the hybrid material, showing the potential of the proposed material to be implemented as a cost-effective optical amplifier for VLC based on white light-emitting diodes.

METHODS

Materials. Poly(propylene glycol)-*block*-poly(ethylene glycol)-*block*-poly(propylene glycol)-*bis*-(2-aminopropyl ether) (Jeffamine ED-600), 3-isocyanatoproplytriethoxysilane (ICPTES), ethanol (high-performance liquid chromatography (HPLC) grade), hydrochloric acid (37% Puriss), potassium bromide (Fourier transform infrared grade), acetonitrile (HPLC grade), and 1,4-dioxane (HPLC grade) were purchased from Sigma-Aldrich and used as received. Tetrahydrofuran (THF) (99.9%) was obtained from Fischer Scientific and used as received. Poly[9,9-bis(4-sulfonylbutoxyphenyl)fluorene-2,7-diyl-*alt*-1,4-phenylene] (PBS-PFP) with an M_n of 6500 g mol^{-1} by gel permeation chromatography (~740 g mol^{-1} repeat units) was a kind gift from Dr. Ana-Teresa Marques and Prof. Ullrich Scherf at Bergische Universität Wuupertal and was synthesized as previously reported.[42]

Synthesis of PBS-PFP Diureasils. PBS-PFP diureasil composites were prepared via the previously reported direct insertion method.[22] This method involves mixing a fixed volume of a stock solution of PBS-PFP in 1,4-dioxane/water (25:75 v/v) with a diureapropyltriethoxysilane (d-UPTES) precursor solution, before inducing acid-catalyzed hydrolysis and condensation of the siliceous backbone to obtain the final PBS-PFP diureasil composite. The d-UPTES precursor was obtained by dissolving Jeffamine ED-600 (1 mL, 1.75 mmol) in THF (5 mL), to which ICPTES (0.9 mL, 3.0 mmol) was added under stirring. This mixture was refluxed at 70 °C for 24 h to obtain the d-UPTES precursor solution. The required volume of the PBS-PFP stock solution was then added to obtain the required PBS-PFP wt % in the final material. In the case of the undoped reference diureasil (denoted as dU(600)),

DOI: 10.1021/acsomega.8b01726
ACS Omega 2018, 3, 13772−13781

an analogous volume of solvent (1,4-dioxane/water (25:75 v/v)) was added for consistency. The sol−gel reaction was triggered by the addition of ethanol (0.409 mL, 7 mmol), HCl (0.5 M, 0.040 mL), and H_2O (0.095 mL, 5.3 mmol) to the d-UPTES solution. This corresponds to a ratio of 1 ICPTES:2.3 EtOH:1.8 H_2O:0.006 HCl molar equivalents. The samples were prepared as either freestanding monoliths or thin films. To obtain the monoliths, the solution containing the gelation agents was transferred into a polypropylene mold, which was then covered with Parafilm M. After 24 h, Parafilm M was pierced to encourage slow evaporation of the solvent, after which it was placed in an oven at 40 °C for 48 h to complete the drying process, producing a freestanding, transparent monolith (∼3 mm thick). PBS-PFP-dU(600) films were prepared by spin-coating a fixed volume of the solution onto SiO_2/Si (300 nm thick SiO_2 layer) substrates. The spin rate was varied to change the film thickness ($\sim 10^1$ μm). The samples are designated as PBS*x*-M or PBS*x*-F for monoliths and films, respectively. The weight percent (wt %) of PBS-PFP incorporated in each sample is indicated in Table 1, and further information of the specific sample thicknesses can be found in Table S1 (Supporting Information, SI).

Production of Channel Waveguides. Linear waveguides were patterned on the surface of the monoliths by direct laser writing, using an UV pulsed laser (Coherent Bragg-Star Industrial V2.0) operating at 248 nm with a frequency of 900 Hz, focused through an objective lens (Thorlabs, LMU-15X-248). The monolith was moved by a PC-controlled stage (Newport, XPS and MFA-CC) at a translation velocity of 0.1 mm s^{-1} on the double-axis translation system. For each monolith, five different waveguides were written with energies of 30, 60, 80, 100, 120 μJ $pulse^{-1}$.

Optical Characterization. *UV/Vis Absorption Spectroscopy.* UV−vis−NIR absorption spectra were recorded at room temperature, using a dual-beam Lambda 950 spectrometer (PerkinElmer) with a 150 mm diameter Spectralon integrating sphere or STD detector module over the scan range (250−1600 nm) and a resolution of 2 nm. The absorption coefficient (α, cm^{-1}) was estimated for all of the monoliths using the Beer−Lambert equation ($\alpha = A/t$, where A and t are the absorbance and thickness, respectively, of each sample).

Photoluminescence Spectroscopy. The emission and excitation spectra were recorded at room temperature using a FluoroLog3 Horiba Scientific (model FL3-2T) spectroscope, with a modular double-grating excitation spectrometer (fitted with a 1200 grooves mm^{-1} grating blazed at 330 nm) and a TRIAX 320 single emission monochromator (fitted with a 1200 grooves mm^{-1} grating blazed at 500 nm, reciprocal linear density of 2.6 nm mm^{-1}), coupled to a R928 photomultiplier (visible measurements), using the front-face acquisition mode. The excitation source was a 450 W Xe arc lamp. The emission spectra were corrected for detection and optical spectral response of the spectrofluorimeter, and the excitation spectra were corrected for the spectral distribution of the lamp intensity using a photodiode reference detector.

Absolute Emission Quantum Yield. The absolute photoluminescence quantum yield (PLQY) values were measured at room temperature using a C9920-02 Hamamatsu system. The method is accurate within 10%.

Spectroscopic Ellipsometry. Spectroscopic ellipsometry measurements were performed using a Horiba Scientific AutoSE spectroscopic ellipsometer at an incidence angle of 69.8°, and an average of 30 measurements per point, for the spectral region between 400 and 850 nm. A measurement spot area of 2.50 × 2.50 ($\times 10^{-4}$ m^2) was used. On the basis of the layered structure, a model consisting of a four-layered system incorporating two layers for the substrate (Si/SiO_2), the doped diureasil layer and air as the ambient medium was considered in the ellipsometric data analysis, for the thin-film samples. The data were minimized using the Simplex algorithm, and the dispersion curves were determined using the Cauchy absorbent model, which expresses the refractive index (n) as a function of the wavelength (λ) described by

$$n(\lambda) = A + \frac{B \times 10^4}{\lambda^2} + \frac{C \times 10^9}{\lambda^4} \quad (3)$$

where A, B, and C are constants and the wavelength is expressed in μm. The reported values for the thickness and refractive index are the average of three measurements performed for each sample with a maximum standard deviation of 5%. For the monoliths with thickness higher than 10^{-5} m, the samples were considered as bulk materials, and the data were minimized using the direct inversion technique, through the above-mentioned Cauchy absorbent model.

Variable Stripe Length Gain Measurement. The optical gain was measured using the variable stripe length (VSL) method. A narrow stripe on the sample surface was optically excited and the amplified spontaneous emission (ASE) signal intensity (I_{ASE}) was collected from the edge of the sample as a function of the stripe length (L).[49] To have a narrow stripe on the sample surface with a variable length, a slit (aperture of 1.5 × 10^{-3} m) and a movable shutter connected to two translation stages (Thorlabs, 13 mm) were used, allowing the stripe length to be controlled within the limits $2.5 \geq L \geq 0$ ($\times 10^{-2}$ m). To detect the I_{ASE}, an optical fiber (Quartz fiber, SMA MMF) and a spectrometer (MAYA Pro 2000, Oceans Optics) were used. The emission spectra were acquired with an integration time of 5 s and 15 scans excited with a UV pump (Vilber VL-6.LC) emitting at 365 nm.

Optical Net Gain Measurements. The optical net gain of the channel waveguide was measured in the spectral domain for a continuous wave diode laser emitting at 450 nm (Roithner LD 450-1600MG). The experimental setup used is represented in Figure 7. The laser signal was coupled to an optical fiber aligned with the channel waveguide using a positioning system (Thorlabs, NanoMax-TS). The propagated signal was collected at the channel output using the above-mentioned positioning system and spectrometer, with an integration time of 10^{-2} s and an average of five scans.

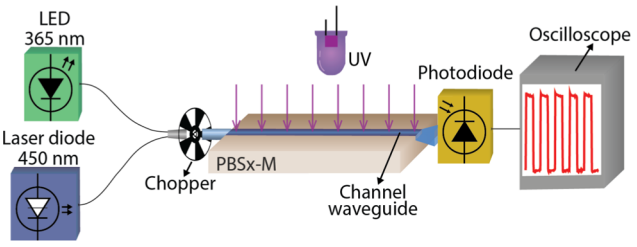

Figure 7. Scheme of the experimental setup used to measure the net gain with a modulated optical signal for the two pumping strategies (external perpendicular or co-propagating).

The net gain was also measured in the time domain using a modulated optical signal, pulsed with a mechanical chopper (MC1F10HP, Thorlabs). For this characterization, the wave-

DOI: 10.1021/acsomega.8b01726
ACS Omega 2018, 3, 13772−13781

guide output optical signal was aligned to a photodiode (DET210, Thorlabs), connected to an oscilloscope (MSO7014B, Agilent Technologies). These measurements were performed under daylight and for two independent optical pumping (UV excitation) configurations: (i) externally to the channel using a UV pump (VL-6.LC, Vilber) as an external waveguide perpendicular pumping architecture or (ii) with an optical signal from a UV-emitting diode (MCLS LED 365, Ocean Optics), injected in the channel input as a co-propagation pumping architecture. This pumping solution provides a compact and integrated system.

■ ASSOCIATED CONTENT

Supporting Information

The Supporting Information is available free of charge on the ACS Publications website at DOI: 10.1021/acsomega.8b01726.

More details on the sample synthesis and processing, spectroscopic ellipsometry analysis, and optical gain measurements (PDF)

■ AUTHOR INFORMATION

Corresponding Author

*E-mail: rferreira@ua.pt. Phone: +351 234 378103.

ORCID

Luís D. Carlos: 0000-0003-4747-6535
Rachel C. Evans: 0000-0003-2956-4857
Rute A. S. Ferreira: 0000-0003-1085-7836

Author Contributions

A.B. produced the channel waveguides by UV laser direct writing and performed the optical characterization measurements. L.D.C., R.C.E., and R.A.S.F. interpreted the photoluminescence data, and P.S.A. and M.L. discussed the optical properties. B.M. and R.C.E synthesized the diureasil organic–inorganic hybrids doped with PBS-PFP. P.S.A. conceived the application for VLC. P.S.A., L.D.C., R.C.E., and R.A.S.F. conceived the approach and supervised the work.

Notes

The authors declare no competing financial interest.

■ ACKNOWLEDGMENTS

The authors acknowledge the Portuguese funds through FCT—Fundação para a Ciência e a Tecnologia, for financially supporting this research under the scope of Instituto de Telecomunicações/IT (UID/EEA/50008/2013) and CICECO-Aveiro Institute of Materials, POCI-01-0145-FEDER-007679 (FCT ref UID/CTM/50011/2013), financed by national funds through the FCT/MEC and when appropriate co-financed by FEDER under the PT2020 Partnership Agreement and project WinLED, no. 030351 (CENTRO-01-0145-FEDER-030351). A.B. acknowledges FCT for the grant PD/BD/105859/2014 (MAP-TELE) and Fundação Calouste Gulbenkian for the "Prémio de Estímulo à Investigação 2015" (Proc no. 141767). This work was supported in part by the Science Foundation Ireland under Grant No. 12/IP/1608. The authors thank Dr. Ana-Teresa Marques and Prof. Ullrich Scherf for the provision of the PBS-PFP conjugated polyelectrolyte.

■ REFERENCES

(1) Pust, P.; Schmidt, P. J.; Schnick, W. A Revolution in Lighting. *Nat. Mater.* **2015**, *14*, 454–458.

(2) Grobe, L.; Paraskevopoulos, A.; Hilt, J.; Schulz, D.; Lassak, F.; Hartlieb, F.; Kottke, C.; Jungnickel, V.; Langer, K.-D. High-Speed Visible Light Communication Systems. *IEEE Commun. Mag.* **2013**, *51*, 60–66.

(3) Zhou, Z.; Tian, P.; Liu, X.; Mei, S.; Zhou, D.; Li, D.; Jing, P.; Zhang, W.; Guo, R.; Qu, S.; et al. Hydrogen Peroxide-Treated Carbon Dot Phosphor with a Bathochromic-Shifted, Aggregation-Enhanced Emission for Light-Emitting Devices and Visible Light Communication. *Adv. Sci.* **2018**, *5*, No. 1800369.

(4) Mei, S.; Liu, X.; Zhang, W.; Liu, R.; Zheng, L.; Guo, R.; Tian, P. High-Bandwidth White-Light System Combining a Micro-LED with Perovskite Quantum Dots for Visible Light Communication. *ACS Appl. Mater. Interfaces* **2018**, *10*, 5641–5648.

(5) Forrest, S. R. The Path to Ubiquitous and Low-Cost Organic Electronic Appliances on Plastic. *Nature* **2004**, *428*, 911–918.

(6) OLED Light, 2018. http://www.lgdisplay.com/eng/product/oled_light.jsp (accessed May 23, 2018).

(7) A New TV Experience Awakens, 2018. https://www.sony.co.uk/electronics/televisions/af8-series (accessed May 23, 2018).

(8) Tan, S. T.; Sun, X. W.; Demir, H. V.; DenBaars, S. P. Advances in the LED Materials and Architectures for Energy-Saving Solid-State Lighting Toward "Lighting Revolution". *IEEE Photonics J.* **2012**, *4*, 613–619.

(9) Hide, F.; Kozodoy, P.; DenBaars, S. P.; Heeger, A. J. White Light from InGaN/Conjugated Polymer Hybrid Light-Emitting Diodes. *Appl. Phys. Lett.* **1997**, *70*, 2664–2666.

(10) Sajjad, M. T.; Manousiadis, P. P.; Chun, H.; Vithanage, D. A.; Rajbhandari, S.; Kanibolotsky, A. L.; Faulkner, G.; O'Brien, D.; Skabara, P. J.; Samuel, I. D. W.; et al. Novel Fast Color-Converter for Visible Light Communication Using a Blend of Conjugated Polymers. *ACS Photonics* **2015**, *2*, 194–199.

(11) Vithanage, D. A.; Kanibolotsky, A. L.; Rajbhandari, S.; Manousiadis, P. P.; Sajjad, M. T.; Chun, H.; Faulkner, G. E.; O'Brien, D. C.; Skabara, P. J.; Samuel, I. D. W.; et al. Polymer Colour Converter with Very High Modulation Bandwidth for Visible Light Communications. *J. Mater. Chem. C* **2017**, *5*, 8916–8920.

(12) Chun, H.; Rajbhandari, S.; Faulkner, G.; O'Brien, D. In *Effectiveness of Blue-Filtering in WLED Based Indoor Visible Light Communication*, 2014 3rd International Workshop in Optical Wireless Communications (IWOW), 2014; pp 60–64.

(13) Karl, M.; Glackin, J. M. E.; Schubert, M.; Kronenberg, N. M.; Turnbull, G. A.; Samuel, I. D. W.; Gather, M. C. Flexible and Ultra-Lightweight Polymer Membrane Lasers. *Nat. Commun.* **2018**, *9*, No. 1525.

(14) Enami, Y.; Derose, C. T.; Mathine, D.; Loychik, C.; Greenlee, C.; Norwood, R. A.; Kim, T. D.; Luo, J.; Tian, Y.; Jen, A. K.-Y.; et al. Hybrid Polymer/Sol–Gel Waveguide Modulators with Exceptionally Large Electro-Optic Coefficients. *Nat. Photonics* **2007**, *1*, 180–185.

(15) Amarasinghe, D.; Ruseckas, A.; Turnbull, G. A.; Samuel, I. D. W. Organic Semiconductor Optical Amplifiers. *Proc. IEEE* **2009**, *97*, 1637–1650.

(16) Clark, J.; Bazzana, L.; Bradley, D. D. C.; Cabanillas-Gonzalez, J.; Lanzani, G.; Lidzey, D. G.; Morgado, J. M.; Nocivelli, A.; Tsoi, W. C.; Virgili, T.; et al. Blue Polymer Optical Fiber Amplifiers Based on Conjugated Fluorene Oligomers. *J. Nanophotonics* **2008**, *2*, No. 023504.

(17) Amarasinghe, D.; Ruseckas, A.; Vasdekis, A. E.; Turnbull, G. A.; Samuel, I. D. W. High-Gain Broadband Solid-State Optical Amplifier Using a Semiconducting Copolymer. *Adv. Mater.* **2008**, *21*, 107–110.

(18) Smirnov, J. R. C.; Zhang, Q.; Wannemacher, R.; Wu, L.; Casado, S.; Xia, R.; Rodriguez, I.; Cabanillas-González, J. Flexible All-Polymer Waveguide for Low Threshold Amplified Spontaneous Emission. *Sci. Rep.* **2016**, *6*, No. 34565.

(19) Sun, L.; Dang, S.; Yu, J.; Feng, J.; Shi, L.; Zhang, H. Near-Infrared Luminescence from Visible-Light-Sensitized Hybrid Materials Covalently Linked with Tris(8-Hydroxyquinolinate)-Lanthanide

DOI: 10.1021/acsomega.8b01726
ACS Omega 2018, 3, 13772–13781

[Er(III), Nd(III), and Yb(III)] Derivatives. *J. Phys. Chem. B* **2010**, *114*, 16393−16397.
(20) Sun, L.-N.; Zhang, H.-J.; Fu, L.-S.; Liu, F.-Y.; Meng, Q.-G.; Peng, C.-Y.; Yu, J.-B. A New Sol−Gel Material Doped with an Erbium Complex and Its Potential Optical-Amplification Application. *Adv. Funct. Mater.* **2005**, *15*, 1041−1048.
(21) Tamai, Y.; Ohkita, H.; Benten, H.; Ito, S. Exciton Diffusion in Conjugated Polymers: From Fundamental Understanding to Improvement in Photovoltaic Conversion Efficiency. *J. Phys. Chem. Lett.* **2015**, *6*, 3417−3428.
(22) Willis-Fox, N.; Marques, A.-T.; Arlt, J.; Scherf, U.; Carlos, L. D.; Burrows, H. D.; Evans, R. C. Synergistic Photoluminescence Enhancement in Conjugated Polymer-Di-Ureasil Organic−inorganic Composites. *Chem. Sci.* **2015**, *6*, 7227−7237.
(23) Willis-Fox, N.; Kraft, M.; Arlt, J.; Scherf, U.; Evans, R. C. Tunable White-Light Emission from Conjugated Polymer-Di-Ureasil Materials. *Adv. Funct. Mater.* **2015**, *26*, 532−542.
(24) Carlos, L. D.; Ferreira, R. A. S.; Pereira, R. N.; Assunção, M.; de Zea Bermudez, V. White-Light Emission of Amine-Functionalized Organic/Inorganic Hybrids: Emitting Centers and Recombination Mechanisms. *J. Phys. Chem. B* **2004**, *108*, 14924−14932.
(25) Fu, L.; Ferreira, R. A. S.; Fernandes, M.; Nunes, S. C.; de Zea Bermudez, V.; Hungerford, G.; Rocha, J.; Carlos, L. D. Photoluminescence and Quantum Yields of Organic/Inorganic Hybrids Prepared through Formic Acid Solvolysis. *Opt. Mater.* **2008**, *30*, 1058−1064.
(26) Ferreira, R. A. S.; Brites, C. D. S.; Vicente, C. M. S.; Lima, P. P.; Bastos, A. R. N.; Marques, P. G.; Hiltunen, M.; Carlos, L. D.; André, P. S. Photonic-on-a-Chip: A Thermal Actuated Mach-Zehnder Interferometer and a Molecular Thermometer Based on a Single Di-Ureasil Organic-Inorganic Hybrid. *Laser Photonics Rev.* **2013**, *7*, 1027−1035.
(27) Vicente, C. M. S.; Lima, P. P.; de Zea Bermudez, V.; Carlos, L. D.; André, P. S.; Ferreira, R. A. S. Fabrication of Low-Cost Thermo-Optic Variable Wave Plate Based on Waveguides Patterned on Di-Ureasil Hybrids. *Opt. Express* **2014**, *22*, 27159−27168.
(28) Vicente, C. M. S.; Venkatachaam, R.; Ferreira, B. M.; Marques, P. G.; Marques, C. A. F.; Pecoraro, E.; Carlos, L. D.; André, P. S.; Ferreira, R. A. S. Thin Film Optimization Design of Organic-Inorganic Hybrids for Waveguide High-Rejection Optical Filters. *Phys. Status Solidi RRL* **2011**, *5*, 280−282.
(29) Kaniyoor, A.; McKenna, B.; Comby, S.; Evans, R. C. Design and Response of High-Efficiency, Planar, Doped Luminescent Solar Concentrators Using Organic−Inorganic Di-Ureasil Waveguides. *Adv. Opt. Mater.* **2015**, *4*, 444−456.
(30) Meazzini, I.; Blayo, C.; Arlt, J.; Marques, A.-T.; Scherf, U.; Burrows, H. D.; Evans, R. C. Ureasil Organic−inorganic Hybrids as Photoactive Waveguides for Conjugated Polyelectrolyte Luminescent Solar Concentrators. *Mater. Chem. Front.* **2017**, *1*, 2271−2282.
(31) Nolasco, M. M.; Vaz, P. M.; Freitas, V. T.; Lima, P. P.; André, P. S.; Ferreira, R. A. S.; Vaz, P. D.; Ribeiro-Claro, P.; Carlos, L. D. Engineering Highly Efficient Eu(III)-Based Tri-Ureasil Hybrids toward Luminescent Solar Concentrators. *J. Mater. Chem. A* **2013**, *1*, 7339.
(32) Correia, S. F. H.; Frias, A. R.; Fu, L.; Rondão, R.; Pecoraro, E.; Ribeiro, S. J. L.; André, P. S.; Ferreira, R. A. S.; Carlos, L. D. Large-Area Tunable Visible-to-Near-Infrared Luminescent Solar Concentrators. *Adv. Sustainable Syst.* **2018**, No. 1800002.
(33) Frias, A. R.; Pecoraro, E.; Correia, S. F. H.; Minas, L. M. G.; Bastos, A. R.; Garcia-Revilla, S.; Balda, R.; Ribeiro, S. J. L.; Andre, P. S.; Carlos, L. D.; et al. Sustainable Luminescent Solar Concentrators Based on Organic-Inorganic Hybrids Modified with Chlorophyll. *J. Mater. Chem. A* **2018**, *6*, 8712−8723.
(34) Ferreira, R. A. S.; André, P. S.; Carlos, L. D. Organic−inorganic Hybrid Materials towards Passive and Active Architectures for the next Generation of Optical Networks. *Opt. Mater.* **2010**, *32*, 1397−1409.
(35) Carlos, L. D.; de Zea Bermudez, V.; Ferreira, R. A. S.; Marques, L.; Assunção, M. Sol−Gel Derived Urea Cross-Linked Organically Modified Silicates. 2. Blue-Light Emission. *Chem. Mater.* **1999**, *11*, 581−588.
(36) Scherf, U.; List, E. J. W. Semiconducting Polyfluorenes—Towards Reliable Structure-Property Relationships. *Adv. Mater.* **2002**, *14*, 477−487.
(37) Wu, H.; Zhang, X.; Guo, C.; Xu, J.; Wu, M.; Su, Q. Three-Band White Light from InGaN-Based Blue LED Chip Precoated with Green/Red Phosphors. *IEEE Photonics Technol. Lett.* **2005**, *17*, 1160−1162.
(38) George, N. C.; Denault, K. A.; Seshadri, R. Phosphors for Solid-State White Lighting. *Annu. Rev. Mater. Res.* **2013**, *43*, 481−501.
(39) Graffion, J.; Cojocariu, A. M.; Cattoën, X.; Ferreira, R. A. S.; Fernandes, V. R.; André, P. S.; Carlos, L. D.; Man, M. W. C.; Bartlett, J. R. Luminescent Coatings from Bipyridine-Based Bridged Silsesquioxanes Containing Eu^{3+} and Tb^{3+} Salts. *J. Mater. Chem.* **2012**, *22*, 13279.
(40) Graffion, J.; Cattoën, X.; Man, M. W. C.; Fernandes, V. R.; André, P. S.; Ferreira, R. A. S.; Carlos, L. D. Modulating the Photoluminescence of Bridged Silsesquioxanes Incorporating Eu^{3+}-Complexed n,n′-Diureido-2,2′-Bipyridine Isomers: Application for Luminescent Solar Concentrators. *Chem. Mater.* **2011**, *23*, 4773−4782.
(41) Pecoraro, E.; Ferreira, R. A. S.; Molina, C.; Ribeiro, S. J. L.; Messsaddeq, Y.; Carlos, L. D. Photoluminescence of Bulks and Thin Films of Eu^{3+}-Doped Organic/Inorganic Hybrids. *J. Alloys Compd.* **2008**, *451*, 136−139.
(42) Burrows, H. D.; Lobo, V. M. M.; Pina, J.; Ramos, M. L.; de Melo, J. S.; Valente, A. J. M.; Tapia, M. J.; Pradhan, S.; Scherf, U. Fluorescence Enhancement of the Water- Soluble Poly{1,4-Phenylene-[9,9-Bis- (4-Phenoxybutylsulfonate)]Fluorene-2,7-Diyl} Copolymer in n-Dodecylpentaoxyethylene Glycol Ether Micelles. *Macromolecules* **2004**, *37*, 7425−7427.
(43) Burrows, H. D.; Tapia, M. J.; Fonseca, S. M.; Valente, A. J. M.; Lobo, V. M. M.; Justino, L. L. G.; Qiu, S.; Pradhan, S.; Scherf, U.; Chattopadhyay, N.; et al. Aqueous Solution Behavior of Anionic Fluorene-Co-Thiophene-Based Conjugated Polyelectrolytes. *ACS Appl. Mater. Interfaces* **2009**, *1*, 864−874.
(44) Evans, R. C.; Macedo, A. G.; Pradhan, S.; Scherf, U.; Carlos, L. D.; Burrows, H. D. Fluorene Based Conjugated Polyelectrolyte/Silica Nanocomposites: Charge-Mediated Phase Aggregation at the Organic-Inorganic Interface. *Adv. Mater.* **2010**, *22*, 3032−3037.
(45) Evans, R. C.; Marr, P. C. Chain Confinement Promotes *β*-Phase Formation in Polyfluorene-Based Photoluminescent Ionogels. *Chem. Commun.* **2012**, *48*, 3742−3744.
(46) Gonçalves, M. C.; Silva, N. J. O.; de Zea Bermudez, V.; Sá Ferreira, R. A.; Carlos, L. D.; Dahmouche, K.; Santilli, C. V.; Ostrovskii, D.; Vilela, I. C. C.; Craievich, A. F. Local Structure and Near-Infrared Emission Features of Neodymium-Based Amine Functionalized Organic/Inorganic Hybrids. *J. Phys. Chem. B* **2005**, *109*, 20093−20104.
(47) Yi, J.; Niu, Q.; Xu, W.; Hao, L.; Yang, L.; Chi, L.; Fang, Y.; Huang, J.; Xia, R. Significant Lowering Optical Loss of Electrodes via Using Conjugated Polyelectrolytes Interlayer for Organic Laser in Electrically Driven Device Configuration. *Sci. Rep.* **2016**, *6*, No. 25810.
(48) Ferreira, R. A. S.; André, P. S.; Carlos, L. D. Organic−inorganic Hybrid Materials towards Passive and Active Architectures for the next Generation of Optical Networks. *Opt. Mater.* **2010**, *32*, 1397−1409.
(49) Negro, L. D.; Bettotti, P.; Cazzanelli, M.; Pacifici, D.; Pavesi, L. Applicability Conditions and Experimental Analysis of the Variable Stripe Length Method for Gain Measurements. *Opt. Commun.* **2004**, *229*, 337−348.
(50) Heliotis, G.; Bradley, D. D. C.; Turnbull, G. A.; Samuel, I. D. W. Light Amplification and Gain in Polyfluorene Waveguides. *Appl. Phys. Lett.* **2002**, *81*, 415−417.
(51) Xia, R.; Heliotis, G.; Hou, Y.; Bradley, D. D. C. Fluorene-Based Conjugated Polymer Optical Gain Media. *Org. Electron.* **2003**, *4*, 165−177.

DOI: 10.1021/acsomega.8b01726
ACS Omega 2018, 3, 13772−13781

(52) Lam, S. Y.; Damzen, M. J. Characterisation of Solid-State Dyes and Their Use as Tunable Laser Amplifiers. *Appl. Phys. B* **2003**, *77*, 577−584.
(53) Rabbani-Haghighi, H.; Forget, Ś; Ch́nais, Ś; Siove, A.; Castex, M. C.; Ishow, E. Laser Operation in Nondoped Thin Films Made of a Small-Molecule Organic Red-Emitter. *Appl. Phys. Lett.* **2009**, *95*, No. 033305.
(54) Mohan, D.; Gaur, A.; Sharma, A. K.; Singh, R. D. Photoquenching in Laser Grade Dyes: Part I. *J. Lumin.* **1989**, *43*, 363−368.
(55) Zenz, C.; Graupner, W.; Tasch, S.; Leising, G.; Iskra, K.; Flieser, J.; Neger, T. Highly Directional Stimulated Emission from a Polymer Waveguide. *J. Appl. Phys.* **1998**, *84*, 5445−5450.
(56) McGehee, M.; Gupta, R.; Veenstra, S.; Miller, E.; Díaz-García, M.; Heeger, A. Amplified Spontaneous Emission from Photopumped Films of a Conjugated Polymer. *Phys. Rev. B* **1998**, *58*, 7035−7039.

DOI: 10.1021/acsomega.8b01726
ACS Omega 2018, 3, 13772−13781